Time scales in shear banding of wormlike micelles

O. Radulescu[1], P. D. Olmsted[2], J. P. Decruppe[3], S. Lerouge[4], J.-F. Berret[5] and G. Porte[5]

[1] *IRMAR - Université de Rennes1, Campus de Beaulieu, 35042, Rennes, France*
[2] *Dept. of Physics and Astronomy, University of Leeds, Leeds LS2 9JT, UK*
[3] *LPLI - Université de Metz, Metz, France*
[4] *LBHP - Université de Paris 7, 2, place Jussieu, 75251 Paris 05, France*
[5] *GDPC - Université de Montpellier II,Montpellier,France*

PACS. 47.50.+d – Non-Newtonian fluid flows.
PACS. 83.10.Tv – Rheology, Structural and phase changes.
PACS. 83.80.Qr – Surfactant and micellar systems, associated polymers.

Abstract. – Transient stress and birefringence measurements are performed on wormlike micellar solutions that "shear band", *i.e.* undergo flow-induced coexistence of states of different viscosities along a constant stress "plateau". Three well defined relaxation times are found after a strain rate step between two banded flow states on the stress plateau. Using the Johnson-Segalman model we relate these time scales to three qualitatively different stages in the evolution of the bands and the interface between them: band destabilization, reconstruction of the interface, and travel of the fully formed interface. The longest timescale is then used to estimate the magnitude of the (unknown) "gradient" terms that must be added to constitutive relations to explain the history independence of the steady flow and the plateau stress selection.

Introduction. – Unlike most fluids, wormlike micelle solutions often have non-analytic measured flow curves with sharply-selected plateaus along which strain rate or stress apparently change discontinuously. In the well-documented shear thinning solutions the usual explanation of the constant stress plateau is shear banding [1–5], *i.e.* a partitioning of the material into bands of different viscosities, triggered by a constitutive instability (such as an isotropic-to-nematic transition [2]). As shown recently [6–10], the stress selection and history independence of shear banding can be explained by incorporating inhomogeneities ("gradient terms" or "diffusion") of the relevant mesoscopic order parameter (polymer stress) in the constitutive equations. Order parameter diffusion has been used since the van der Waals "gradient theory" of the gas-liquid interface [11] and is obligatory in phase field models for pattern formation. Notwithstanding a few attempts to deal with inhomogeneous stresses [12], the same concepts are largely absent from the rheological literature. While one might argue that gradient, or diffusion, terms are negligibly small, these *singular* terms resolve stress selection even for infinitesimal values [7–9]. However, a small diffusion coefficient should also imply a slow approach to steady state; the main purpose of this letter is to demonstrate these long time scales experimentally.

TABLE I – *Systems used in this study; the surfactant was* 0.3 M *CTAB.* τ *and* G_0*, are the Maxwell relaxation time and modulus,* $\dot{\gamma}_c, \delta\dot{\gamma}$ *are the start and width of the constant stress plateau,* $(\tau_i)_{i=1,3}$ *are the three time scales discussed in the text, and* σ^* *is the plateau stress.*

No.	Salt	$T/^o$C	G_0/Pa	τ/s	τ_1/s	τ_2/s	τ_3/s	$\tau\dot{\gamma}_c$	$\tau\delta\dot{\gamma}$	σ^*/G_o
1	1.79M $NaNO_3$	30	232	0.17	0.2	1.1	31	0.85	19	0.64
2	0.405M $NaNO_3$	30	238	0.17	0.2	1.8	27	1.27	19	0.66
3	0.3M KBr	34	235	0.16	0.2	1.9	13	1.12	80	0.66

Shear banding involves spatial inhomogeneity and temporal dynamics. We use light polarization to probe the spatial inhomogeneity and its dynamics, and rheology to measure the time evolution of the total stress. The stress transients are also computed using a theoretical model. Rather than the typical start-up transient experiment, we consider the simpler experiment of a step between two values of the shear rate in the banded regime. Small steps should induce less drastic changes in the fluid while still remaining in the non-linear regime and hopefully yield more controllable results. The transient features will be shown to be intimately related to the dynamics of the interface between the bands.

Experiments. – The surfactant solutions are summarized in Table I. The stress was measured using an RFS Rheometrics Scientific controlled shear rate ($\dot{\gamma}$) rheometer in Couette (radii 24.5, 25 mm) and cone-plate geometries. Linear response is of the Maxwell type with almost identical relaxation times τ and moduli G_0 for the three solutions. In the non-linear regime shear banding occurs at $\dot{\gamma}_c$ and the plateau width is $\dot{\gamma}_N - \dot{\gamma}_I \equiv \delta\dot{\gamma}$ (See Refs. [1, 2] for experimental flow curves, or Fig. 2 for a schematic representation). The plateau is wider and flatter for solution 3 than for solutions 1 and 2, for which it roughly follows a power law $\sigma \sim \dot{\gamma}^\alpha, \alpha \lesssim 0.1$; a slope could indicate concentration differences between coexisting bands [13]. Upon a step increase of the mean shear rate from $\dot{\gamma}_1$ to $\dot{\gamma}_2$ (both on the plateau) the stress increases and then decreases monotonically (or sometimes by a small undershoot and a monotonic increase). A semi-log plot of the stress vs. time shows that three relaxation times ($\tau_1 \approx \tau \approx 10^{-1}$ s, $\tau_2 \approx 10\tau$, $\tau_3 \approx 100\tau$) follow successively until steady flow is reached (Fig. 1a). Although the overshoot is present for very small steps, distinct time scales are poorly defined. For optimal choices of the initial and final conditions ($\dot{\gamma}_1 \approx \dot{\gamma}_c$ and $(\dot{\gamma}_2 - \dot{\gamma}_1) \ll \delta\dot{\gamma}$) the three time scales are well separated and the result is reproducible for all solutions and both cone-plate and Couette geometries. We filmed the step shear rate experiment for the third solution in a Couette geometry with a slightly larger gap (radii 24, 25 mm) between crossed polarizers. The birefringence contrast in Fig. 4 shows the bands (the nematic, high shear, band is bright([1])). An average extinction angle χ has also been extracted. The kinetics of χ displays a time scale similar but slightly shorter than τ_2 measured by rheology (Fig. 1c). We cannot expect to resolve a first time scale as in rheology, because this is shorter than the video frame interval. The third time scale is buried in noise not confidently extractable.

Theory. – The momentum balance is $\rho\,(\partial_t + \boldsymbol{v}\cdot\boldsymbol{\nabla})\,\boldsymbol{v} = \boldsymbol{\nabla}\cdot\boldsymbol{T}$, where ρ is the fluid density and $\boldsymbol{v}$ is the velocity field. The stress tensor $\boldsymbol{T}$ is given by $\boldsymbol{T} = -p\,\boldsymbol{I} + 2\eta\boldsymbol{A} + \boldsymbol{\Sigma}$, where the pressure p is determined by incompressibility ($\boldsymbol{\nabla}\cdot\boldsymbol{v} = 0$), η is the "solvent" viscosity, $\boldsymbol{\Sigma}$ is the "polymer" stress, and $\boldsymbol{A}$ is the symmetric part of the velocity gradient tensor $(\boldsymbol{\nabla}\boldsymbol{v})_{\alpha\beta} \equiv \partial_\alpha v_\beta$. The non-Newtonian "polymer" viscoelastic stress $\boldsymbol{\Sigma}$ is assumed to obey the diffusive Johnson-Segalman (d-JS) model [7],

$$(\partial_t + \boldsymbol{v}\cdot\boldsymbol{\nabla})\,\boldsymbol{\Sigma} - (\boldsymbol{\Omega}\boldsymbol{\Sigma} - \boldsymbol{\Sigma}\,\boldsymbol{\Omega}) - a\,(\boldsymbol{A}\boldsymbol{\Sigma} + \boldsymbol{\Sigma}\boldsymbol{A}) = \mathcal{D}\nabla^2\boldsymbol{\Sigma} + 2\mu\boldsymbol{A}/\tau - \boldsymbol{\Sigma}/\tau, \qquad (1)$$

([1])For a different system ref. [14] argued that the more birefringent band is not always of highest shear rate.

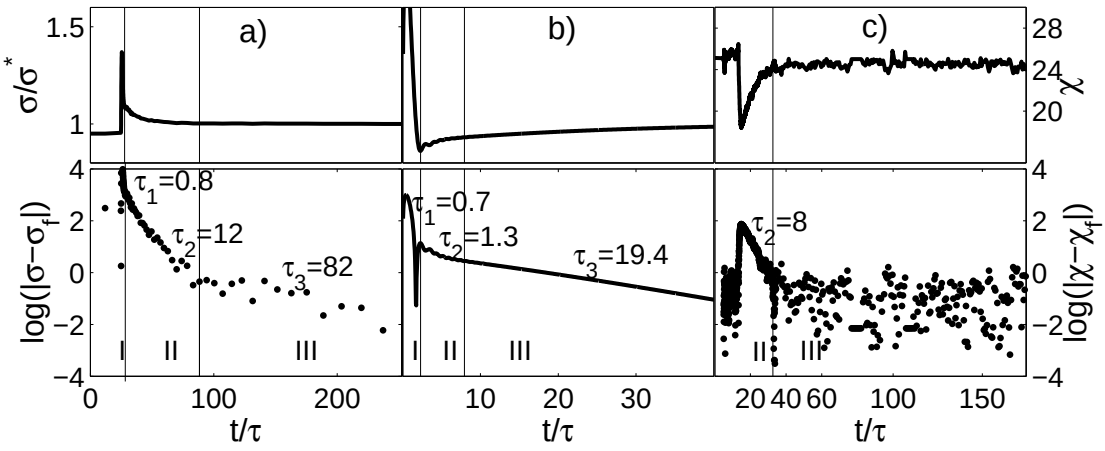

Fig. 1 – Total stress (a) and extinction angle (c) during the step $\dot{\gamma} = 10 \rightarrow 20\ s^{-1}$ for CTAB/KBr; (b) simulated total stress for the step $\dot{\gamma}\tau = 1.2 \rightarrow 3.9$ using the d-JS model ($\epsilon = 0.03$, $D\tau/L^2 = 5 \cdot 10^{-5}$)

where $\boldsymbol{\Omega}$ is the anti-symmetric part of $\boldsymbol{\nabla v}$, $\mu = G_o\tau$ is the "polymer" viscosity, τ is a relaxation time, and $\mathcal{D}$ is the diffusion coefficient. The "slip parameter" a (describing the non-affinity of the deformation) is necessary to reproduce a non-monotonic constitutive curve and the added diffusion term was shown to resolve stress selection [7].

The initial dynamics is governed by inertia; within a short time $\tau_\rho = \rho L^2/\eta$ ($= 10^{-4}$ s for $\eta/\rho = 0.01\,\mathrm{m^2 s^{-1}}$ and gap $L = 1$ mm) the strain rate homogenizes and the momentum balance becomes $\boldsymbol{T} = const.$ The subsequent dynamics is controlled by the viscoelastic response. In a planar geometry, $\boldsymbol{v} = v(y)\hat{\boldsymbol{x}}$, Eq. (1) leads to a system of reaction-diffusion equations([2]):

$$\frac{\partial S}{\partial t} = \mathcal{D}\frac{\partial^2 S}{\partial y^2} - \frac{S}{\tau} + C_S(\dot{\gamma}, S, W), \qquad \frac{\partial W}{\partial t} = \mathcal{D}\frac{\partial^2 W}{\partial y^2} - \frac{W}{\tau} + C_W(\dot{\gamma}, S, W), \tag{2}$$

where $\dot{\gamma}$ is the shear rate, $S = \Sigma_{xy}$, and W is a combination of the polymer normal stresses, Σ_{xx} and Σ_{yy}. S, W are the order parameters of the transition (S is small in the nematic (N) band and large in the isotropic (I) band). They can diffuse across stream lines with diffusion coefficient $\mathcal{D}$ and relax in the linear regime within the linear (Maxwell) time τ. The reaction terms $C_S = \dot{\gamma}(G_o - W)$ and $C_W = \dot{\gamma}S$ can be straightforwardly derived from Eq. (1) [6,8].

The local momentum balance for the shear stress $\sigma = T_{xy}$ is

$$\sigma = S + \epsilon G_o \tau \dot{\gamma}, \tag{3}$$

where $\epsilon = \eta/\mu$. Two dynamical systems are important for the understanding of the local nonlinear dynamics of Eq. 2:

$$\dot{S} = -S/\tau + C_S(\dot{\gamma}, S, W), \qquad \dot{W} = -W/\tau + C_W(\dot{\gamma}, S, W); \tag{4a}$$

$$\dot{S} = -S/\tau + C_S((\sigma - S)/\epsilon G_0\tau, S, W), \qquad \dot{W} = -W/\tau + C_W((\sigma - S)/\epsilon G_0\tau, S, W) \tag{4b}$$

where $\dot{S} \equiv \partial S/\partial t$. System (4a) describes the dynamics along a streamline at prescribed shear rate; in this case σ changes proportionately to S according to Eq. (3). System (4b) describes

([2])Any non-monotonic differential constitutive model (*e.g.* Cates [17], Doi-Edwards [15, 16]) with diffusion terms leads to a similar equation set.

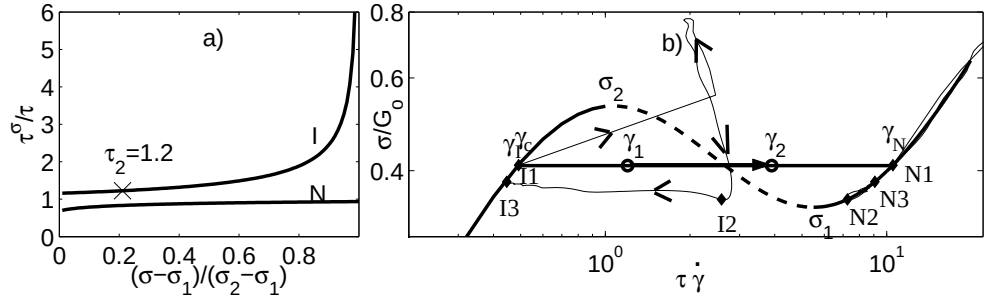

Fig. 2 – a) Relaxation times to I and N attractors at constant stress for d-JS model, $\tau_I^\sigma, \tau_N^\sigma$; τ_2 corresponds to σ at the end of stage 2 in the simulation, to compare with the fitted value in Fig. 1b. b) Thick line: theoretical flow curve (the negative-slope unstable branch is experimentally resolved by the constant stress plateau). Thin lines: simulated trajectories of material near the walls, representing the N and I bands. $\{N_i, I_i\}, i = 1, 2, 3$ denote the beginnings of the three relaxation stages.

the dynamics along a streamline at constant total stress σ. The two dynamical systems have the same fixed points (since, for homogeneous steady flow, $\dot{\gamma}$ and σ are related by Eq. 3): stable fixed points (attractors) representing the bands I and N, and an intermediate unstable saddle. Coexistence of bands at common total stress is possible only for $\sigma \in [\sigma_1(\epsilon), \sigma_2(\epsilon)]$. Linearizing systems (4a) and (4b) about the fixed points yields the dominant relaxation times of the attractors, τ_I and τ_N. These are different for the two dynamical systems, denoted at constant shear rate by $\tau^\gamma_{I,N}$ and at constant stress by $\tau^\sigma_{I,N}$. For the JS model $\tau^\gamma_I = \tau^\gamma_N = \tau$ for all $\dot{\gamma}$. τ^σ_N is close to τ, while τ^σ_I is larger than τ^σ_N and diverges as $\sigma \to \sigma_2(\epsilon)$ (Fig. 2a). This divergence is consistent with Ref. [5]: controlled stress experiments have increasing relaxation times on the metastable extension of the I branch above the constant stress plateau.

Consider an initial banded steady state, with average shear rate $\dot{\gamma}_1$. Suddenly increasing the average shear rate to $\dot{\gamma}_2$ produces a stress overshoot because the amount of low viscosity N band can not change instantly; after the overshoot the stress will decrease by production of the low viscosity N material. Numerical simulation (Figs. 1b, 3) shows that this occurs in three stages:

1. Band I destabilization— During this stage the I band tries a direct passage toward the nematic band N, Fig. 3a. Complete transformation is forbidden by the average shear rate constraint and the I band stops before reaching the basin of attraction of the steady N band. A representation of the subsequent kinetics in the $(\dot{\gamma}, \sigma)$ plane (Fig. 2b) shows that *the N band almost follows the steady flow curve, while the I band evolves at constant shear rate.* Thus, the characteristic time $\tau_1 \approx \tau^\gamma_I \approx \tau$ is controlled by the I band dynamics.

2. Interface reconstruction— At the end of stage 1 an interface separates the locally unstable band close to the saddle from the locally stable N band. The part of the unstable band closer to the I attractor will return to this, while the other part will go to the N attractor. This reconstructs the interface in a more advanced position, stabilizes the bands, and increases the contrast between them. The stress variation is much smaller than during the first stage. The sign of this variation depends on the initial stress for this stage, which is sensitive to the details of the constitutive model. If this stress is below the plateau (the stress drop after the overshoot is strong in stage 1) then a stress increase follows (as in Fig. 1b). The experimental situation corresponds to a smaller stress drop in the first stage and a monotonic stress after the overshoot (Fig. 1a). Nevertheless, the time scale (controlled by the I band) $\tau_2 \approx \tau^\sigma_I$ depends only on the final stress and is thus not affected by the presence

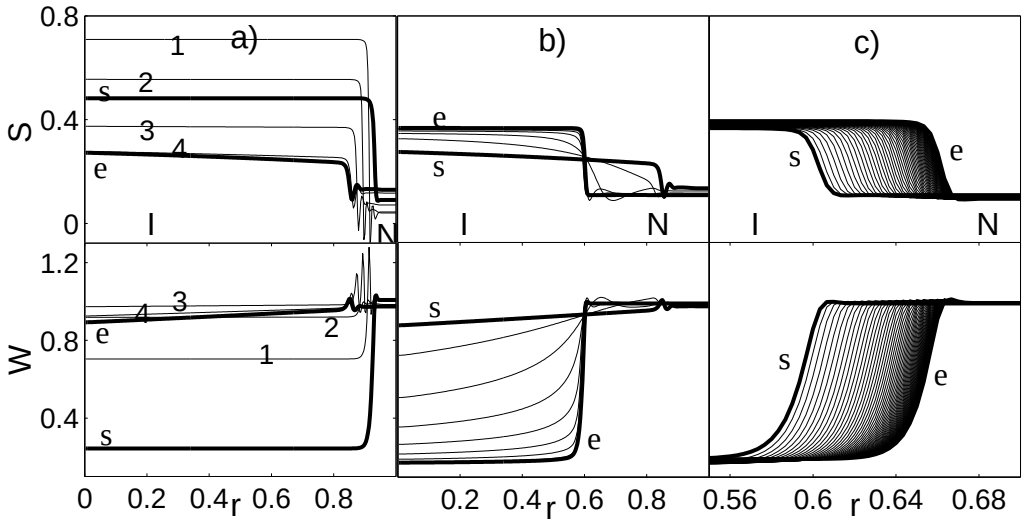

Fig. 3 – Simulation of the order parameter profiles for the three stages (s: start, e: end): a) destabilization ($0 < t < t_1$); b) reconstruction ($t_1 < t < t_2$); c) travel ($t_2 < t < \infty$).

or absence of an undershoot as long as the stress variation during this stage is small. This analysis is compatible with the birefringence measurements. The sequence of images in Fig. 4 shows the gap of the Couette cell filmed between crossed polarizers during stage 2. Although we can not quantitatively compare Figs. 3b and 4 (the relation between the transmitted intensity and the order parameter is unknown and sure to be non-linear), the sharpening of the contrast corresponding to the interface reconstruction is visible. The difference between the characteristic times for the extinction angle and rheology (Fig.1) could be due either to the different cell gap widths or to errors in the exponential fit (notoriously unstable).

3. Interface travel— The instability and reconstruction of the interface in the first two stages is ensured by the reaction terms of Eq. (2), ending when the interface between stable bands fully sharpens. This interface has a non-zero velocity if it forms at a position corresponding to a stress value above or below the plateau stress σ^*. *Front propagation* over the small distance toward the final equilibrium position is then controlled by $\mathcal{D}$ (this distance is too small to observe by birefringence). Because of the undershoot in the numerical simulation the sign of the displacement during stage 3 is opposite to the one in the first stages (Fig. 3c). The characteristic time τ_3 for this stage follows from the velocity c of the sharp interface close to steady state, which is *history independent* (see below).

Let us consider a single sharp interface, at a position r inside the gap. At imposed shear rate $\dot{\gamma}_2$, the lever rule $\dot{\gamma}_2 = \frac{r}{L}\dot{\gamma}_N(\sigma) + (1 - \frac{r}{L})\dot{\gamma}_I(\sigma)$ relates σ and r and leads to

$$\left(\frac{\partial \sigma}{\partial r}\right)_{\langle\dot{\gamma}\rangle} = -\frac{\eta_I \dot{\gamma}_I \delta\dot{\gamma}}{L\dot{\gamma}_2}, \tag{5}$$

where $\delta\dot{\gamma} = \dot{\gamma}_N - \dot{\gamma}_I$ is the width of the plateau, and $\eta_I = \partial\sigma/\partial\dot{\gamma}|_{\dot{\gamma}_I}$. As discussed in [5–7], because of metastability (like in equilibrium liquid-gas transitions) the isotropic band shear rate $\dot{\gamma}_I$ could be slightly smaller than the transition rate $\dot{\gamma}_c$. We consider $\dot{\gamma}_2 - \dot{\gamma}_I \ll \delta\dot{\gamma}$, $\delta\dot{\gamma} \gg \dot{\gamma}_I$ (as in the experiments) so that $\eta_I\dot{\gamma}_I \approx \eta_N\delta\dot{\gamma}$ (true for piecewise linear flow curves and obeyed well by the JS model).

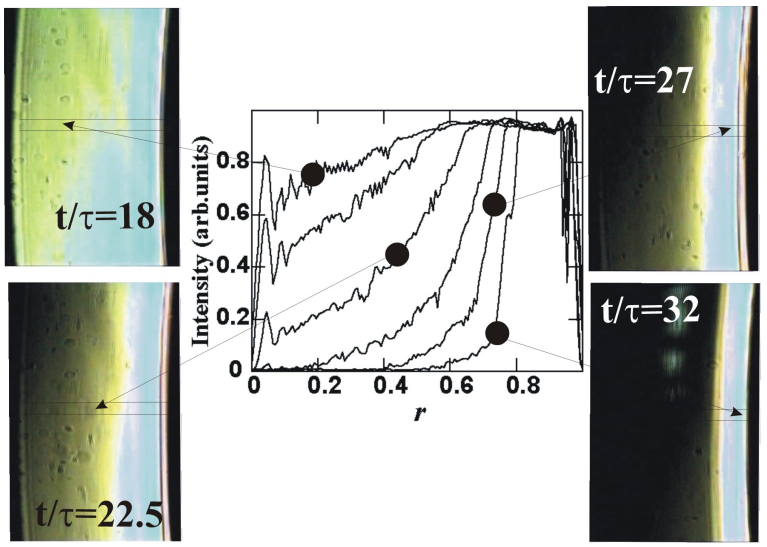

Fig. 4 – CTAB/KBr: $\dot{\gamma} = 10 \rightarrow 30s^{-1}$ jump: birefringence images and profiles (averaged between the two vertical lines on the film) corresponding to Stage 2, interfacial reconstruction. The moving (inner) cylinder is at $r = 1.0$ and the fixed (outer) cylinder is at $r = 0.0$.

We showed previously that the velocity c of the interface is a function only of the total shear stress σ and that $c = 0$ when $\sigma = \sigma^*$ [6,8] which, via the lever rule, corresponds to a unique stable interface position r^*. Close to r^* the equation of motion of the interface is:

$$\frac{dr}{dt} = c(\sigma) = \frac{dc}{d\sigma}\left(\frac{\partial\sigma}{\partial r}\right)_{\langle\dot{\gamma}\rangle}(r - r^*). \tag{6}$$

Using Eqs. (5,6), $\frac{d\sigma}{dc}\big|_{\sigma=\sigma^*} \equiv KG_o\sqrt{\frac{\tau}{\mathcal{D}}}$ (K is a dimensionless parameter depending on the constitutive model), we find the solution $r - r^* = (r(0) - r^*)e^{-t/\tau_3}$, where:

$$\tau_3 = \tau\frac{L}{\sqrt{\mathcal{D}\tau}}\frac{KG_o\tau}{\eta_I\dot{\gamma}_I}\frac{\dot{\gamma}_2}{\delta\dot{\gamma}}, \tag{7}$$

Eq. (7) implies that a fully formed interface equilibrates faster in systems with larger plateaus $\delta\dot{\gamma}$, such as CTAB/KBr. In such cases, Eq. (5) implies larger stress variations and thus larger interface accelerations for the same position variation. This is compatible with the shorter τ_3 in Table I. For simplicity, Eq. (5) was found for a planar geometry; in cylindrical Couette flow a slight correction (negligible for thin gaps as here) leads to a smaller τ_3.

Using the experimental value of τ_3 and Eq. (7), we can estimate $\mathcal{D}$. Generally, we need the value of K. In the d-JS model, while G_0 and τ are measurable, K depends on the two free parameters ϵ and a. Nevertheless, when these parameters change, $\frac{KG_o\tau}{\eta_I\dot{\gamma}_I} \approx 0.3-0.4$ practically stays constant ([3]) and $\mathcal{D}$ can be obtained without the knowledge of a or ϵ. Microscopically, we expect $\mathcal{D} = \zeta^2/\tau$ where ζ is the stress correlation length. In dilute solutions this should be the micelle gyration radius [12], while in concentrated solutions a reasonable candidate is the mesh size ξ, which can be estimated from $G_o \sim kT/\xi^3$. The results are presented in Table II.

([3])Appropriate scaling shows the independence of a; the weak dependence on ϵ was checked numerically for the d-JS model

No.	L/mm	$\dot{\gamma}_2/\delta\dot{\gamma}$	$\mathcal{D}/(\mathrm{m^2 s^{-1}})$	ζ/nm	ξ/nm
1	0.3	0.22	$7.2\,10^{-14}$	111	26
2	0.3	0.18	$6.1\,10^{-14}$	100	26
3	0.3	0.04	$1.2\,10^{-14}$	44	26

TABLE II – Stress diffusion estimates using the JS model. $\mathcal{D}$ is obtained from the values of τ_3 (table I) and Eq. 7 with $\frac{KG_o\tau}{\eta_I\dot{\gamma}_I} = 0.3$.

The stress correlation length is of order the mesh size, which is reasonable; however there is still no theory for such a diffusive term in concentrated solutions.

To conclude, a general dynamical systems analysis of the d-JS model provides plausible explanations for the observed time scales and consistent estimates of the stress diffusion coefficient $\mathcal{D}$. The analysis is illustrated by a numerical simulation that uses optimal parameters. Without entering into details that are left for future study, non-optimal parameters (too large or too small jumps, values of ϵ,$\mathcal{D}$) may lead to poorly separated time scales or to damped but visible stress oscillations that are not observed experimentally. The reason to postpone these details is that neither the d-JS nor reptation-reaction models [16, 17] can provide perfect fits of the transient stress of wormlike micelles and there is still a need for the suitable constitutive model. Also, it it conceivable that concentration differences between the bands could influence the observed time scales which is consistent with the values of $\mathcal{D}$ in Table II (similar for the samples 1,2, significantly smaller for the sample 3 for which the plateau is flat and presumably concentrations effects are weak).

* * *

We thank J.-F.Tassin for his kind assistance and for allowing our access to the rheometer facilities of Université du Maine. O.R. acknowledges funding from EU COST Action P1 on Soft Condensed Matter and from EPSRC (GR/L70455) at the beginning of this work.

REFERENCES

[1] REHAGE H. and HOFFMANN H. , *J. Phys.Chem.*, **92** (1988) 4712.
[2] BERRET J.-F., ROUX D. C. and PORTE G., *J. Phys. II (France)*, **4** (1994) 1261.
[3] SPENLEY N. A., CATES M. E. and MCLEISH T. C. B., *Phys. Rev. Lett*, **71** (1993) 939.
[4] BERRET J.-F., *Langmuir*, **13** (1997) 2227.
[5] GRAND C., ARRAULT J. and CATES M. E., *J. Phys. II (France)*, **7** (1997) 1071.
[6] RADULESCU O., OLMSTED P. D. and LU C.-Y. D., *Rheol. Acta*, **38** (1999) 606.
[7] OLMSTED P. D., RADULESCU O. and LU C.-Y. D., *J. Rheol.*, **44** (2000) 257.
[8] RADULESCU O. and OLMSTED P. D. , *J. Non-Newtonian Fluid Mech.*, **91** (2000) 141.
[9] LU C.-Y. D., OLMSTED P. D. and R. C. BALL, *Phys. Rev. Lett.*, **84** (2000) 642.
[10] YUAN X. F, *Europhys. Lett.*, **46** (1999) 542; DHONT J., *Phys. Rev.*, **E60** (1999) 4534.
[11] VAN DER WAALS J. D., *Verh. Konink. Akad. Wetensch. Amsterdam*, **1** (1893) 1071, translated in ROWLINSON J. S., *J. Stat. Phys.*, **20** (1979) 197.
[12] EL-KAREH A. W. and LEAL L. G., *J. Non-Newtonian Fluid Mech.*, **33** (1989) 257.
[13] SCHMITT V., MARQUES, C. M. and LEQUEUX, F., *Phys. Rev.*, **E52** (1995) 4009; OLMSTED P. D. and LU C.-Y. D., *Phys. Rev.*, **E56** (1997) 55.
[14] FISCHER E. and CALLAGHAN P. T., *Europhys. Lett.*, **50** (2000) 803.
[15] LARSON R. G., *Constitutive Equations for Polymer Melts and Solutions* (Butterworth, Guildford) 1988.
[16] DOI M. and EDWARDS S. F., *The Theory of Polymer Dynamics* (Clarendon, Oxford) 1986.
[17] CATES M. E. , *J. Phys. Chem.*, **94** (1990) 371.